Smart Structures and Systems, *Vol. 24, No. 4 (2019) 459-474*
DOI: https://doi.org/10.12989/sss.2019.24.4.459

A novel recursive stochastic subspace identification algorithm with its application in long-term structural health monitoring of office buildings

Wen-Hwa Wu*, Jhe-Wei Jhou[a], Chien-Chou Chen[b] and Gwolong Lai[c]

Department of Construction Engineering, National Yunlin University of Science and Technology, 123 University Road, Douliu, Yunlin 640, Taiwan

(Received January 11, 2019, Revised June 20, 2019, Accepted June 23, 2019)

Abstract. This study develops a novel recursive algorithm to significantly enhance the computation efficiency of a recently proposed stochastic subspace identification (SSI) methodology based on an alternative stabilization diagram. Exemplified by the measurements taken from the two investigated office buildings, it is first demonstrated that merely one sixth of computation time and one fifth of computer memory are required with the new recursive algorithm. Such a progress would enable the realization of on-line and almost real-time monitoring for these two steel framed structures. This recursive SSI algorithm is further applied to analyze 20 months of monitoring data and comprehensively assess the environmental effects. It is certified that the root-mean-square (RMS) response can be utilized as an excellent index to represent most of the environmental effects and its variation strongly correlates with that of the modal frequency. More detailed examination by comparing the monthly correlation coefficient discloses that larger variations in modal frequency induced by greater RMS responses would typically lead to a higher correlation.

Keywords: stochastic subspace identification; recursive algorithm; alternative stabilization diagram; structural health monitoring; office building; environmental effect

1. Introduction

The modal identification and structural health monitoring (SHM) of large-scale civil structures have been more popularly conducted with ambient vibration measurements because of the advantages in easy operation and low cost. State-of-the-art review of recent works on signal processing techniques for vibration-based SHM was also presented (Amezquita-Sanchez and Adeli 2016). Because simply the output signals are available in these applications, the output-only or operational modal analysis (OMA) is required to effectively obtain the modal frequencies, damping ratios, and mode shape vectors. Several OMA methods either via the frequency domain or the time domain analysis or both have been developed with the research progress in the past few decades. Among all these output-only identification techniques, stochastic subspace identification (SSI) has drawn particular attentions in civil and infrastructure engineering applications (He *et al*. 2008, Reynders and De Roeck 2008, Hu *et al*. 2010, Whelam and Janoyan 2010, Foti *et al*. 2014) owing to its relatively solid mathematical basis and wide applicability. Since the commonly employed formulation of SSI was first proposed (Van Overschee and De Moor 1991), the corresponding algorithm by directly processing the output matrix from measurements for modal parameter identification was subsequently established (Van Overschee and De Moor 1993, Van Overschee and De Moor 1996) and usually referred as the data-driven SSI. A number of techniques in linear algebra such as LQ (or QR) decomposition, singular value decomposition (SVD), and oblique projection were adopted in the data-driven SSI to enhance the reliability of solutions. Other than the series of data-driven methods, the covariance-driven type (Van Overschee and De Moor 1996) was also developed to implement SSI by the covariance matrix of output measurements with the benefits in simpler mathematical derivation and computation efficiency.

Even though rapidly growing in recent years, the applications of SSI techniques in civil structures such as bridges and buildings still face a few practical difficulties. One of the most critical problems is that obtained modal parameters can be varied by selecting different values of the time lag parameter and the system order parameter, both necessary to be prescribed in conducting the SSI analysis. The stabilization diagram is customarily used to overcome this difficulty by displaying the gradually increased system order along the ordinate and the corresponding modal frequencies along the abscissa under an assigned value of the time lag parameter. It is expected that the actual physical modes can be clearly distinguished by stable frequency values concentrated at separated narrow strips. Moreover, appropriate discrimination criteria based on theories like clustering analysis (Scionti and Lanslots 2005, Carden and Brownjohn 2008, Bakir 2011) need to be established such that systematic extraction of effective

*Corresponding author, Professor
E-mail: wuwh@yuntech.edu.tw
[a] Former Graduate Student
[b] Professor
[c] Associate Professor

ISSN: 1738-1584 (Print), 1738-1991 (Online)

physical modes and an automated SSI analysis (Magalhaes *et al*. 2009, Reynders *et al*. 2012, Ubertini *et al*. 2013) can be attained. Further consideration of computation efficiency is also required if the ultimate goal is aimed for online and real-time health monitoring of civil structures. Certain recursive algorithms for data-driven SSI (Loh *et al*. 2011, Weng and Loh 2011, Loh *et al*. 2013) were accordingly suggested to simplify the LQ (or QR) decomposition and SVD operations for the updated measurements by fully exploiting the decomposed results before the inclusion of new signals. Lately, the recursive algorithms for covariance-driven SSI (Li and Chang 2012, Loh and Liu 2013, Liu *et al*. 2013) have also been developed to deal with the covariance matrix incorporating the new outputs.

Since the civil structures are usually subjected to nonstationary excitations, the selection of a fixed time lag parameter to construct the conventional stabilization diagram may still have a strong influence on the determined modal parameters (Magalhaes *et al*. 2009, Wu *et al*. 2016a). Specific heuristic rules were utilized in the literature such as the one that the time lag parameter should cover an adequately large number of cycles of the lowest frequency (Magalhaes *et al*. 2009, Ubertini *et al*. 2013). Recent works by the authors (Wu *et al*. 2016a, Wu *et al*. 2017a) further attempted to verify that the lower limit of time lag parameter for steady modal identification results can be decided by the ratio of the fundamental period of structure to the sampling time increment in several types of structures. Following this criterion, a new methodology based on the covariance-driven SSI was proposed by introducing an alternative stabilization diagram to exhibit the results with varying values of the time lag parameter for more conveniently distinguishing stable modal parameters (Wu *et al*. 2016a, Wu *et al*. 2016b). A hierarchical sifting process was also devised to automatically extract consistent modal parameters from the alternative stabilization diagram consisting of three sequential stages (Wu *et al*. 2016a).

With the above improved SSI algorithm, accurate and continuous identification of modal parameters based on long-term vibration measurements was further conducted for cable-stayed bridges (Wu *et al.* 2017b, Wu *et al.* 2019) and office buildings (Wu *et al.* 2017c, Wu *et al*. 2019) to investigate the environmental effects in SHM. It has been well recognized that the effect of environmental factors may also induce considerable variations of structural responses and modal parameters in addition to material degradation and structural damages. Therefore, assessment of environmental effects is undoubtedly a pivotal component for the success of vibration-based SHM approaches applied to civil structures. Several recent works have examined the influences of various environmental factors such as temperature, traffic load, and wind speed on long-span bridges (Cao *et al*. 2011, Li *et al.* 2014). The environmental temperature and the passing traffic have been found to play the dominant roles for the modal frequency variations of either cable-stayed bridges (Zhang *et al*. 2002, Macdonald and Daniell 2005, Min *et al*. 2009, Sun *et al*. 2015) or suspension bridges (Apaydin *et al*. 2012, Westgate *et al*. 2015). However, relatively few works evaluated the environmental effects of building structures and most of them focused on heritage arenas (Lorenzoni *et al*. 2016), historic churches (Ramos *et al*. 2010, Gentile and Saisi 2013), ancient towers (Ramos *et al*. 2010, Gentile and Saisi 2013, Saisi *et al*. 2015, Saisi *et al*. 2016, Ubertini *et al*. 2017), or modern high towers (Faravelli *et al*. 2011). From these studies, it has been observed that the frequencies of globally bending modes for a historic church or an ancient tower typically increase with the increasing environmental temperature (Ramos *et al*. 2010, Saisi *et al*. 2015, Saisi *et al*. 2016, Ubertini *et al*. 2017) and the trend is opposite for local modes (Saisi *et al*. 2016) or globally torsional modes (Ubertini *et al*. 2017). Besides, the higher excitation intensity (response level) (Gentile and Saisi 2013) or the increasing air humidity (Ramos *et al*. 2010) is likely to reduce the modal frequencies of these structures. Regarding the modern high towers, it was discovered that the rising temperature would generally correspond to declined modal frequencies (Faravelli *et al*. 2011).

Recent attention has been paid to the environmental effects on modern building structures and it was revealed that their modal frequencies correlate to the environmental temperature (Yuen and Kuok 2010) with certain time delays (Nayeri *et al*. 2008). Furthermore, investigations based on the real vibration measurements of modern buildings also indicated that the increasing excitation intensity would normally decrease the modal frequencies (Faheem and Piotr 2014) and may increase the corresponding damping ratios (Faheem and Piotr 2014, Belleri *et al*. 2014). More recently, the work by the authors (Wu *et al*. 2017c) conducted a long-term identification for the modal parameters of two instrumented office buildings using ambient vibration measurements. The analyzed results unveiled that the modal frequencies of both buildings highly correlate with the root-mean-square (RMS) vibration response in a negative manner and the corresponding damping ratios also hold a positive correlation. The above success is majorly due to the accurate identification contributed by the special ingredients of alternative stabilization diagram and hierarchical sifting process in the new SSI algorithm. Nevertheless, it should be especially emphasized that such a reliable method comes with the price of more intensive computation. The current study is consequently targeted on further removing this crucial obstacle in realistic SHM applications by the development of a novel recursive formula to prominently improve the computation efficiency of SSI analysis. Making use of the recursive SSI algorithm, an extended analysis covering 20 months of monitoring data for the observed office buildings is carried out in this work to comprehensively investigate the environmental effects and demonstrate the feasibility of on-line SHM.

2. Stochastic subspace identification based on alternative stabilization diagram

In this section, the procedures of the covariance-driven stochastic subspace identification and the concepts of alternative stabilization diagram are briefly reviewed to serve as the backgrounds for developing a recursive algorithm presented in the next section.

2.1 Covariance-driven SSI

The theoretical derivation of SSI methods conventionally starts from the state space description of a linear dynamic system with *n* degrees of freedom (DOF). If the output measurements are conducted with the sampling time increment Δt, the $l \times l$ covariance matrix corresponding to a specified time lag $m\Delta t$ for the $l \times 1$ output vector $\mathbf{y}_k$ at the time instant $k\Delta t$ is defined by

$$\mathbf{H}_m = \mathrm{E}[\mathbf{y}_k \mathbf{y}_{k+m}{}^{\mathrm{T}}] \tag{1}$$

where $\mathrm{E}[\cdot]$ signifies the expected value of the bracketed quantity. Moreover, systematic arrangement of the covariance matrices $\mathbf{H}_m$'s with different time lags from Δt to $(2i-1)\Delta t$ would lead to the so-called Toeplitz matrix associated with the time lag parameter *i*

$$\mathbf{T}^{(i)} = \begin{bmatrix} \mathbf{H}_i & \mathbf{H}_{i-1} & \cdots & \mathbf{H}_1 \\ \mathbf{H}_{i+1} & \mathbf{H}_i & \cdots & \mathbf{H}_2 \\ \vdots & \vdots & \ddots & \vdots \\ \mathbf{H}_{2i-1} & \mathbf{H}_{2i-2} & \mathbf{H}_{i+1} & \mathbf{H}_i \end{bmatrix} \tag{2}$$

which is $il \times il$. Further considering the output vectors measured at *N* consecutive time instants from 0 to $(N-1)\Delta t$, they can be systematically organized into a Hankel matrix with the selection of a time lag parameter *i*

$$\begin{aligned} \mathbf{Y}^{(i)} &= \frac{1}{\sqrt{N-2i+1}} \begin{bmatrix} \mathbf{y}_0 & \mathbf{y}_1 & \cdots & \mathbf{y}_{N-2i} \\ \mathbf{y}_1 & \mathbf{y}_2 & \cdots & \mathbf{y}_{N-2i+1} \\ \vdots & \vdots & \ddots & \vdots \\ \mathbf{y}_{i-1} & \mathbf{y}_i & \cdots & \mathbf{y}_{N-i-1} \\ \hline \mathbf{y}_i & \mathbf{y}_{i+1} & \cdots & \mathbf{y}_{N-i} \\ \mathbf{y}_{i+1} & \mathbf{y}_{i+2} & \cdots & \mathbf{y}_{N-i+1} \\ \vdots & \vdots & \ddots & \vdots \\ \mathbf{y}_{2i-1} & \mathbf{y}_{2i} & \cdots & \mathbf{y}_{N-1} \end{bmatrix}_{2il \times (N-2i+1)} \\ &= \begin{bmatrix} \mathbf{Y}^{(i)}(1:il,:) \\ \hline \mathbf{Y}^{(i)}((il+1):2il,:) \end{bmatrix} \end{aligned} \tag{3}$$

Post-multiplication of $\mathbf{Y}^{(i)}((il+1):2il,:)$ by $\mathbf{Y}^{(i)}(1:il,:)^{\mathrm{T}}$ results in the approximation of Toeplitz matrix $\mathbf{T}^{(i)}$

$$\begin{aligned} \hat{\mathbf{T}}^{(i)} &= \mathbf{Y}^{(i)}((il+1):2il,:)\,\mathbf{Y}^{(i)}(1:il,:)^{\mathrm{T}} \\ &= \frac{1}{N-2i+1} \begin{bmatrix} \sum_{k=0}^{N-2i} \mathbf{y}_{k+i}\mathbf{y}_k^{\mathrm{T}} & \sum_{k=0}^{N-2i} \mathbf{y}_{k+i}\mathbf{y}_{k+1}^{\mathrm{T}} & \sum_{k=0}^{N-2i} \mathbf{y}_{k+i}\mathbf{y}_{k+2}^{\mathrm{T}} & \cdots & \sum_{k=0}^{N-2i} \mathbf{y}_{k+i}\mathbf{y}_{k+i-1}^{\mathrm{T}} \\ \sum_{k=0}^{N-2i} \mathbf{y}_{k+i+1}\mathbf{y}_k^{\mathrm{T}} & \sum_{k=0}^{N-2i} \mathbf{y}_{k+i+1}\mathbf{y}_{k+1}^{\mathrm{T}} & \sum_{k=0}^{N-2i} \mathbf{y}_{k+i+1}\mathbf{y}_{k+2}^{\mathrm{T}} & \cdots & \sum_{k=0}^{N-2i} \mathbf{y}_{k+i+1}\mathbf{y}_{k+i-1}^{\mathrm{T}} \\ \vdots & \vdots & \vdots & \ddots & \vdots \\ \sum_{k=0}^{N-2i} \mathbf{y}_{k+2i-2}\mathbf{y}_k^{\mathrm{T}} & \sum_{k=0}^{N-2i} \mathbf{y}_{k+2i-2}\mathbf{y}_{k+1}^{\mathrm{T}} & \sum_{k=0}^{N-2i} \mathbf{y}_{k+2i-2}\mathbf{y}_{k+2}^{\mathrm{T}} & \cdots & \sum_{k=0}^{N-2i} \mathbf{y}_{k+2i-2}\mathbf{y}_{k+i-1}^{\mathrm{T}} \\ \sum_{k=0}^{N-2i} \mathbf{y}_{k+2i-1}\mathbf{y}_k^{\mathrm{T}} & \sum_{k=0}^{N-2i} \mathbf{y}_{k+2i-1}\mathbf{y}_{k+1}^{\mathrm{T}} & \sum_{k=0}^{N-2i} \mathbf{y}_{k+2i-1}\mathbf{y}_{k+2}^{\mathrm{T}} & \cdots & \sum_{k=0}^{N-2i} \mathbf{y}_{k+2i-1}\mathbf{y}_{k+i-1}^{\mathrm{T}} \end{bmatrix} \\ &\approx \begin{bmatrix} \mathbf{H}_i & \mathbf{H}_{i-1} & \mathbf{H}_{i-2} & \cdots & \mathbf{H}_1 \\ \mathbf{H}_{i+1} & \mathbf{H}_i & \mathbf{H}_{i-1} & \cdots & \mathbf{H}_2 \\ \vdots & \vdots & \vdots & \ddots & \vdots \\ \mathbf{H}_{2i-2} & \mathbf{H}_{2i-3} & \mathbf{H}_{2i-4} & \cdots & \mathbf{H}_{i-1} \\ \mathbf{H}_{2i-1} & \mathbf{H}_{2i-2} & \mathbf{H}_{2i-3} & \cdots & \mathbf{H}_i \end{bmatrix} = \mathbf{T}^{(i)} \end{aligned} \tag{4}$$

It should be noted that stationary zero-mean outputs are typically assumed in the SSI analysis and the number *N* needs to be sufficiently large for the validity of this approximation.

With the approximation of Toeplitz matrix $\hat{\mathbf{T}}^{(i)}$ available, singular value decomposition (SVD) can then be performed to obtain

$$\begin{aligned} \hat{\mathbf{T}}^{(i)} &= \mathbf{U}\mathbf{S}\mathbf{V}^{\mathrm{T}} \\ &= \begin{bmatrix} (\mathbf{U}_1)_{il \times 2n} & (\mathbf{U}_2)_{il \times n_1} \end{bmatrix} \begin{bmatrix} (\mathbf{S}_1)_{2n \times 2n} & \mathbf{0}_{2n \times n_1} \\ \mathbf{0}_{n_1 \times 2n} & (\mathbf{S}_2)_{n_1 \times n_1} \approx \mathbf{0}_{n_1 \times n_1} \end{bmatrix} \begin{bmatrix} (\mathbf{V}_1^{\mathrm{T}})_{2n \times il} \\ (\mathbf{V}_2^{\mathrm{T}})_{n_1 \times il} \end{bmatrix} \\ &\approx \mathbf{U}_1\mathbf{S}_1\mathbf{V}_1^{\mathrm{T}} \end{aligned} \tag{5}$$

where $n_1 = il - 2n$, $\mathbf{U}$ and $\mathbf{V}$ are orthogonal matrices, and $\mathbf{S}$ is a quasi-diagonal matrix with positive diagonal elements sorted in a decreasing order. By taking

$$\mathbf{O}_i = \mathbf{U}_1\mathbf{S}_1^{1/2} \quad \text{and} \quad \mathbf{\Gamma}_i = \mathbf{S}_1^{1/2}\mathbf{V}_1^{\mathrm{T}} \tag{6}$$

from Eq. (5), it has been proved (Peeters 2000) that the discretized system matrix $\mathbf{A}$ in the state space can be solved by

$$\mathbf{A} = \mathbf{O}_i^{\oplus}(1:l(i-1),:)\mathbf{O}_i(l+1:li,:) \tag{7}$$

where $\oplus$ symbolizes the pseudo inverse operation. Based on the theory of linear systems, the modal frequencies ω_k's, the damping ratios ξ_k's, and the mode shape vectors at the output measurement locations $\boldsymbol{\varphi}_k$'s can be subsequently determined from the eigenvalues and eigenvectors of $\mathbf{A}$.

According to the above review, it is evident that the time lag parameter *i* in Eq. (3) and the system order parameter *n* in Eq. (5) have to be prescribed in conducting the covariance-driven SSI analysis. If the excitation is close to the white-noise assumption, the time lag parameter is supposed to be insensitive for the subsequent modal parameters identified from the SSI analysis. Nevertheless, the situation would be alternated when the excitation is narrowly banded in the frequency domain. The system order parameter *n*, on the other hand, designates the largest $2n$ singular values in Eq. (5) to compose the two matrices in Eq. (6) and thus decides the size of the discretized system

matrix **A**. A value of *n* adequately larger than the number of physical modes within the interested frequency range is usually adopted to guarantee the incorporation of sufficient contributing modes. Even though the use of higher model orders can result in the inclusion of spurious numerical modes, it may be helpful to model the noise generally existed in measured data for the identification of weakly excited modes (Magalhaes *et al*. 2009, Ubertini *et al*. 2013).

2.2 Critical threshold for time lag parameter and alternative stabilization diagram

The normally confronted difficulty for the applications of SSI techniques in large-scale civil structures is that the excitation exerted on a real structure and the measurement noise do not actually satisfy all the zero-mean, white-noise, and stationary assumptions on which the derivation of SSI is based. To handle this discrepancy, the SSI technique is regularly applied together with the stabilization diagram in which the system order *n* displayed along the ordinate is gradually increased to identify different sets of modal frequencies plotted along the abscissa under a designated value of *i*. In the stabilization diagram, it is expected that the actual physical modes can be obviously distinguished from the spurious modes by closely clustered frequency values. However, the performance of stabilization diagrams for the applications in civil structures may be still strongly influenced by the choice of time lag parameter.

To cope with the challenge of applying SSI techniques in identifying the parameters for numerous modes of a stay cable, an effort was recently made by the authors to investigate the appropriate selection of time lag parameter (Wu *et al*. 2016a). Because all the modal frequencies of a stay cable are with the values approximately in integer multiples of its fundamental frequency f_1, it was pointed out that the ambient vibration signal of cable would be close to a periodic function with a quasi-period nearly equal to the period $T_1 = 1/f_1$ of the first cable mode. In accordance with Eq. (1), the corresponding covariance matrix $\mathbf{H}_m$ for cable measurements would hold the property of $\mathbf{H}_{m+i} \approx \mathbf{H}_m$ if $i\Delta t$ is equal to the quasi-period T_1 of cable signal. Besides, the matrix structure in Eq. (4) further ensures that all the different patterns of $\mathbf{H}_m$ would be uniformly utilized in the SSI analysis if

$$i \geq i_c = \frac{T_1}{\Delta t} = \frac{s}{f_1} \tag{8}$$

where $s = 1/\Delta t$ represents the sampling rate and i_c means the critical threshold for the time lag parameter to assure stable identification results. Even for the measurements from the other types of civil structures with irregularly distributed modal frequencies (Wu *et al*. 2016b, Wu *et al*. 2017a, Wu *et al*. 2017b, Wu *et al*. 2017c, Wu *et al*. 2019), Eq. (8) was also confirmed to be essentially applicable since the unbiased distribution containing all the independent patterns of $\mathbf{H}_m$ may still be roughly attained in these cases.

Inspired by the important discovery of Eq. (8), the authors further proposed a new concept of alternative stabilization diagram by exhibiting the gradually increased time lag parameter *i* along the ordinate and the corresponding modal frequencies along the abscissa under an assigned value of the system order *n* (Wu *et al*. 2016a). It was suggested to first examine the Fourier amplitude spectra (FAS) of the measurements for choosing the system parameter *n* that is approximately twice of the number for the observable peaks (Ubertini *et al*. 2013). The fundamental period of the investigated structure can also be observed from FAS to determine the lower limit $i_{\min} = i_c$ by Eq. (8). In addition, the upper limit of time lag parameter $i_{\max} = i_{\min} + \Delta i$ is decided by the need in the subsequent processes to obtain consistent modal parameters. Regarding the computational cost, the disadvantage associated with the alternative stabilization diagram is that construction of Hankel matrix in Eq. (3), determination of the approximate Toeplitz matrix in Eq. (4), and SVD operation in Eq. (5) all have to be conducted all over again with each different value of *i*. It should also be noted that the costs for the above operations would increase with the increasing value of *i* due to the enlarged matrix size. As a result, the computation efficiency may become a critical concern for the application of alternative stabilization diagrams in the SSI analysis.

3. Recursive algorithm for alternative stabilization diagram

To substantially reduce the computational cost in constructing the alternative stabilization diagram, a novel approach is developed in this section. The mathematical relation between the two approximate Toeplitz matrices associated with adjacent values of time lag parameter, $\hat{\mathbf{T}}^{(i)}$ and $\hat{\mathbf{T}}^{(i-1)}$, is first derived by deliberately examining the similarity of their matrix structures. Taking advantage of this relationship, a recursive algorithm is then proposed, followed by discussing its computation efficiency.

3.1 Relation between Toeplitz matrices with adjacent values of time lag parameter

For the convenience of further derivation, the expression in Eq. (4) for approximate Toeplitz matrix associated with the time parameter *i* can be rewritten as

$$\begin{aligned}
&\hat{\mathbf{T}}^{(i)} \\
&= \mathbf{Y}^{(i)}\big((il+1):2il,:\big)\,\mathbf{Y}^{(i)}(1:il,:)^{\mathrm{T}} \\
&= \frac{1}{N-2i+1}\begin{bmatrix}
\sum_{k=0}^{N-2i}\mathbf{y}_{k+i}\mathbf{y}_k^{\mathrm{T}} & \sum_{k=1}^{N-2i+1}\mathbf{y}_{k+i-1}\mathbf{y}_k^{\mathrm{T}} & \sum_{k=2}^{N-2i+2}\mathbf{y}_{k+i-2}\mathbf{y}_k^{\mathrm{T}} & \cdots & \sum_{k=i-1}^{N-i-1}\mathbf{y}_{k+1}\mathbf{y}_k^{\mathrm{T}} \\
\sum_{k=0}^{N-2i}\mathbf{y}_{k+i+1}\mathbf{y}_k^{\mathrm{T}} & \sum_{k=1}^{N-2i+1}\mathbf{y}_{k+1}\mathbf{y}_k^{\mathrm{T}} & \sum_{k=2}^{N-2i+2}\mathbf{y}_{k+i-1}\mathbf{y}_k^{\mathrm{T}} & \cdots & \sum_{k=i-1}^{N-i-1}\mathbf{y}_{k+2}\mathbf{y}_k^{\mathrm{T}} \\
\vdots & \vdots & \vdots & \ddots & \vdots \\
\sum_{k=0}^{N-2i}\mathbf{y}_{k+2i-2}\mathbf{y}_k^{\mathrm{T}} & \sum_{k=1}^{N-2i+1}\mathbf{y}_{k+2i-3}\mathbf{y}_k^{\mathrm{T}} & \sum_{k=2}^{N-2i+2}\mathbf{y}_{k+2i-4}\mathbf{y}_k^{\mathrm{T}} & \cdots & \sum_{k=i-1}^{N-i-1}\mathbf{y}_{k+i-1}\mathbf{y}_k^{\mathrm{T}} \\
\sum_{k=0}^{N-2i}\mathbf{y}_{k+2i-1}\mathbf{y}_k^{\mathrm{T}} & \sum_{k=1}^{N-2i+1}\mathbf{y}_{k+2i-2}\mathbf{y}_k^{\mathrm{T}} & \sum_{k=2}^{N-2i+2}\mathbf{y}_{k+2i-3}\mathbf{y}_k^{\mathrm{T}} & \cdots & \sum_{k=i-1}^{N-i-1}\mathbf{y}_{k+1}\mathbf{y}_k^{\mathrm{T}}
\end{bmatrix} \\
&= \frac{1}{N-2i+1}\begin{bmatrix}
\hat{\mathbf{H}}_{i,0}^{(i)} & \hat{\mathbf{H}}_{(i-1),1}^{(i)} & \hat{\mathbf{H}}_{(i-2),2}^{(i)} & \cdots & \hat{\mathbf{H}}_{1,(i-1)}^{(i)} \\
\hat{\mathbf{H}}_{(i+1),0}^{(i)} & \hat{\mathbf{H}}_{i,1}^{(i)} & \hat{\mathbf{H}}_{(i-1),2}^{(i)} & \cdots & \hat{\mathbf{H}}_{2,(i-1)}^{(i)} \\
\vdots & \vdots & \vdots & \ddots & \vdots \\
\hat{\mathbf{H}}_{(2i-2),0}^{(i)} & \hat{\mathbf{H}}_{(2i-3),1}^{(i)} & \hat{\mathbf{H}}_{(2i-4),2}^{(i)} & \cdots & \hat{\mathbf{H}}_{(i-1),(i-1)}^{(i)} \\
\hat{\mathbf{H}}_{(2i-1),0}^{(i)} & \hat{\mathbf{H}}_{(2i-2),1}^{(i)} & \hat{\mathbf{H}}_{(2i-3),2}^{(i)} & \cdots & \hat{\mathbf{H}}_{i,(i-1)}^{(i)}
\end{bmatrix}
\end{aligned} \tag{9}$$

where the $l \times l$ matrix $\hat{\mathbf{H}}_{m,p}^{(i)}$ is defined by

$$\hat{\mathbf{H}}_{m,p}^{(i)} \equiv \sum_{k=p}^{N-2i+p} \mathbf{y}_{k+m}\mathbf{y}_k^{\mathrm{T}}, \quad m = 1, 2, \cdots\cdots, 2i-1 \tag{10}$$

and can be regarded as an estimation of $\mathbf{H}_m$ with the measurements from the time instant $p\Delta t$ to $(N-2i+p)\Delta t$ under the time lag parameter i. The definition of Eq. (10) further yields the following relationship

$$\begin{aligned}\hat{\mathbf{H}}_{m,p+1}^{(i)} &= \sum_{k=p+1}^{N-2i+p+1} \mathbf{y}_{k+m}\mathbf{y}_k^{\mathrm{T}} \\ &= \mathbf{y}_{N-2i+p+1+m}\mathbf{y}_{N-2i+p+1}^{\mathrm{T}} - \mathbf{y}_{p+m}\mathbf{y}_p^{\mathrm{T}} + \sum_{k=p}^{N-2i+j} \mathbf{y}_{k+m}\mathbf{y}_k^{\mathrm{T}} \\ &= \mathbf{y}_{N-2i+p+1+m}\mathbf{y}_{N-2i+p+1}^{\mathrm{T}} - \mathbf{y}_{p+m}\mathbf{y}_p^{\mathrm{T}} + \hat{\mathbf{H}}_{m,p}^{(i)}\end{aligned} \tag{11}$$

Next, consider the case that the time lag parameter is i–1 and its corresponding Hankel matrix becomes

$$\begin{aligned}\mathbf{Y}^{(i-1)} &= \frac{1}{\sqrt{N-2i-3}} \begin{bmatrix} \mathbf{y}_0 & \mathbf{y}_1 & \cdots & \mathbf{y}_{N-2i+2} \\ \mathbf{y}_1 & \mathbf{y}_2 & \cdots & \mathbf{y}_{N-2i+3} \\ \vdots & \vdots & \ddots & \vdots \\ \mathbf{y}_{i-2} & \mathbf{y}_{i-1} & \cdots & \mathbf{y}_{N-i} \\ \hline \mathbf{y}_{i-1} & \mathbf{y}_i & \cdots & \mathbf{y}_{N-i+1} \\ \mathbf{y}_i & \mathbf{y}_{i+1} & \cdots & \mathbf{y}_{N-i+2} \\ \vdots & \vdots & \ddots & \vdots \\ \mathbf{y}_{2i-3} & \mathbf{y}_{2i-2} & \cdots & \mathbf{y}_{N-1} \end{bmatrix} \\ &= \begin{bmatrix} \mathbf{Y}^{(i-1)}(1:(i-1)l,:) \\ \hline \mathbf{Y}^{(i-1)}(i(l-1)+1):2(i-1)l,:) \end{bmatrix}\end{aligned} \tag{12}$$

Similar to the case with the time lag parameter i, the Toeplitz matrix for the time lag parameter i–1 can be approximated by

$$\begin{aligned}\hat{\mathbf{T}}^{(i-1)} &= \mathbf{Y}^{(i-1)}((i-1)l+1):2(i-1)l,:)\mathbf{Y}^{(i-1)}(1:(i-1)l,:)^{\mathrm{T}} \\ &= \frac{1}{N-2i+3} \begin{bmatrix} \sum_{k=0}^{N-2i+2} \mathbf{y}_{k+i-1}\mathbf{y}_k^{\mathrm{T}} & \sum_{k=0}^{N-2i+2} \mathbf{y}_{k+i-1}\mathbf{y}_{k+1}^{\mathrm{T}} & \cdots & \sum_{k=0}^{N-2i+2} \mathbf{y}_{k+i-1}\mathbf{y}_{k+i-2}^{\mathrm{T}} \\ \sum_{k=0}^{N-2i+2} \mathbf{y}_{k+i}\mathbf{y}_k^{\mathrm{T}} & \sum_{k=0}^{N-2i+2} \mathbf{y}_{k+i}\mathbf{y}_{k+1}^{\mathrm{T}} & \cdots & \sum_{k=0}^{N-2i+2} \mathbf{y}_{k+i}\mathbf{y}_{k+i-2}^{\mathrm{T}} \\ \vdots & \vdots & \ddots & \vdots \\ \sum_{k=0}^{N-2i+2} \mathbf{y}_{k+2i-3}\mathbf{y}_k^{\mathrm{T}} & \sum_{k=0}^{N-2i+2} \mathbf{y}_{k+2i-3}\mathbf{y}_{k+1}^{\mathrm{T}} & \cdots & \sum_{k=0}^{N-2i+2} \mathbf{y}_{k+2i-3}\mathbf{y}_{k+i-2}^{\mathrm{T}} \end{bmatrix} \\ &= \frac{1}{N-2i+3} \begin{bmatrix} \sum_{k=0}^{N-2i+2} \mathbf{y}_{k+i-1}\mathbf{y}_k^{\mathrm{T}} & \sum_{k=1}^{N-2i+3} \mathbf{y}_{k+i-2}\mathbf{y}_k^{\mathrm{T}} & \cdots & \sum_{k=i-2}^{N-i} \mathbf{y}_{k+1}\mathbf{y}_k^{\mathrm{T}} \\ \sum_{k=0}^{N-2i+2} \mathbf{y}_{k+i}\mathbf{y}_k^{\mathrm{T}} & \sum_{k=1}^{N-2i+3} \mathbf{y}_{k+i-1}\mathbf{y}_k^{\mathrm{T}} & \cdots & \sum_{k=i-2}^{N-i} \mathbf{y}_{k+2}\mathbf{y}_k^{\mathrm{T}} \\ \vdots & \vdots & \ddots & \vdots \\ \sum_{k=0}^{N-2i+2} \mathbf{y}_{k+2i-3}\mathbf{y}_k^{\mathrm{T}} & \sum_{k=0}^{N-2i+3} \mathbf{y}_{k+2i-3}\mathbf{y}_{k+1}^{\mathrm{T}} & \cdots & \sum_{k=i-2}^{N-i} \mathbf{y}_{k+i-1}\mathbf{y}_k^{\mathrm{T}} \end{bmatrix} \\ &= \frac{1}{N-2i+3} \begin{bmatrix} \hat{\mathbf{H}}_{(i-1),0}^{(i-1)} & \hat{\mathbf{H}}_{(i-2),1}^{(i-1)} & \cdots & \hat{\mathbf{H}}_{1,(i-2)}^{(i-1)} \\ \hat{\mathbf{H}}_{i,0}^{(i-1)} & \hat{\mathbf{H}}_{(i-1),1}^{(i-1)} & \cdots & \hat{\mathbf{H}}_{2,(i-2)}^{(i-1)} \\ \vdots & \vdots & \ddots & \vdots \\ \hat{\mathbf{H}}_{(2i-3),0}^{(i-1)} & \hat{\mathbf{H}}_{(2i-4),1}^{(i-1)} & \cdots & \hat{\mathbf{H}}_{(i-1),(i-2)}^{(i-1)} \end{bmatrix}\end{aligned} \tag{13}$$

where $\hat{\mathbf{T}}^{(i-1)}$ is $(i-1)l \times (i-1)l$ and the $l \times l$ matrix $\hat{\mathbf{H}}_{m,p}^{(i-1)}$ is defined by

$$\hat{\mathbf{H}}_{m,p}^{(i-1)} \equiv \sum_{k=p}^{N-2i+p+2} \mathbf{y}_{k+m}\mathbf{y}_k^{\mathrm{T}}, \quad m = 1, 2, \cdots\cdots, 2i-3 \tag{14}$$

With the definitions of Eqs. (10) and (14), it is found that

$$\begin{aligned}\hat{\mathbf{H}}_{m,p}^{(i-1)} &= \mathbf{y}_{N-2i+p+2+m}\mathbf{y}_{N-2i+p+2}^{\mathrm{T}} + \mathbf{y}_{p+m}\mathbf{y}_p^{\mathrm{T}} + \sum_{k=p+1}^{N-2i+p+1} \mathbf{y}_{k+m}\mathbf{y}_k^{\mathrm{T}} \\ &= \mathbf{y}_{N-2i+p+2+m}\mathbf{y}_{N-2i+p+2}^{\mathrm{T}} + \mathbf{y}_{j+m}\mathbf{y}_p^{\mathrm{T}} + \hat{\mathbf{H}}_{m,p+1}^{(i)}\end{aligned} \tag{15}$$

From Eq. (15), Eq. (13) can be expressed as

$$\begin{aligned}\hat{\mathbf{T}}^{(i-1)} &= \frac{1}{N-2i+3} \left\{ \begin{bmatrix} \hat{\mathbf{H}}_{(i-1),1}^{(i)} & \hat{\mathbf{H}}_{(i-2),2}^{(i)} & \cdots & \hat{\mathbf{H}}_{1,(i-1)}^{(i)} \\ \hat{\mathbf{H}}_{i,1}^{(i)} & \hat{\mathbf{H}}_{(i-1),2}^{(i)} & \cdots & \hat{\mathbf{H}}_{2,(i-1)}^{(i)} \\ \vdots & \vdots & \ddots & \vdots \\ \hat{\mathbf{H}}_{(2i-3),1}^{(i)} & \hat{\mathbf{H}}_{(2i-4),2}^{(i)} & \cdots & \hat{\mathbf{H}}_{(i-1),(i-1)}^{(i)} \end{bmatrix} \right. \\ &\quad + \begin{bmatrix} \mathbf{y}_{i-1}\mathbf{y}_0^{\mathrm{T}} & \mathbf{y}_{i-1}\mathbf{y}_1^{\mathrm{T}} & \cdots & \mathbf{y}_{i-1}\mathbf{y}_{i-2}^{\mathrm{T}} \\ \mathbf{y}_i\mathbf{y}_0^{\mathrm{T}} & \mathbf{y}_i\mathbf{y}_1^{\mathrm{T}} & \cdots & \mathbf{y}_i\mathbf{y}_{i-2}^{\mathrm{T}} \\ \vdots & \vdots & \ddots & \vdots \\ \mathbf{y}_{2i-3}\mathbf{y}_0^{\mathrm{T}} & \mathbf{y}_{2i-3}\mathbf{y}_1^{\mathrm{T}} & \cdots & \mathbf{y}_{2i-3}\mathbf{y}_{i-2}^{\mathrm{T}} \end{bmatrix} \\ &\quad \left. + \begin{bmatrix} \mathbf{y}_{N-i+1}\mathbf{y}_{N-2i+2}^{\mathrm{T}} & \mathbf{y}_{N-i+1}\mathbf{y}_{N-2i+3}^{\mathrm{T}} & \cdots & \mathbf{y}_{N-i+1}\mathbf{y}_{N-i}^{\mathrm{T}} \\ \mathbf{y}_{N-i+2}\mathbf{y}_{N-2i+2}^{\mathrm{T}} & \mathbf{y}_{N-i+2}\mathbf{y}_{N-2i+3}^{\mathrm{T}} & \cdots & \mathbf{y}_{N-i+2}\mathbf{y}_{N-i}^{\mathrm{T}} \\ \vdots & \vdots & \ddots & \vdots \\ \mathbf{y}_{N-1}\mathbf{y}_{N-2i+2}^{\mathrm{T}} & \mathbf{y}_{N-1}\mathbf{y}_{N-2i+3}^{\mathrm{T}} & \cdots & \mathbf{y}_{N-1}\mathbf{y}_{N-i}^{\mathrm{T}} \end{bmatrix} \right\} \\ &= \frac{1}{N-2i+3} \left\{ \begin{array}{l} (N-2i+1)\mathbf{T}^{(i)}(1:(i-1)l,(l+1):il) + \begin{Bmatrix} \mathbf{y}_{i-1} \\ \mathbf{y}_i \\ \vdots \\ \mathbf{y}_{2i-3} \end{Bmatrix} \begin{Bmatrix} \mathbf{y}_0^{\mathrm{T}} & \mathbf{y}_1^{\mathrm{T}} & \cdots & \mathbf{y}_{i-2}^{\mathrm{T}} \end{Bmatrix} \\ + \begin{Bmatrix} \mathbf{y}_{N-i+1} \\ \mathbf{y}_{N-i+2} \\ \vdots \\ \mathbf{y}_{N-1} \end{Bmatrix} \begin{Bmatrix} \mathbf{y}_{N-2i+2}^{\mathrm{T}} & \mathbf{y}_{N-2i+3}^{\mathrm{T}} & \cdots & \mathbf{y}_{N-i}^{\mathrm{T}} \end{Bmatrix} \end{array} \right\} \\ &= \frac{1}{N-2i+3} \left\{ (N-2i+1)\hat{\mathbf{T}}^{(i)}(1:(i-1)l,(l+1):il) + \mathbf{F}^{(i-1)} + \mathbf{B}^{(i-1)} \right\}\end{aligned} \tag{16}$$

where

$$\mathbf{F}^{(i-1)} \equiv \begin{Bmatrix} \mathbf{y}_{i-1} \\ \mathbf{y}_i \\ \vdots \\ \mathbf{y}_{2i-3} \end{Bmatrix} \begin{Bmatrix} \mathbf{y}_0^{\mathrm{T}} & \mathbf{y}_1^{\mathrm{T}} & \cdots & \mathbf{y}_{i-2}^{\mathrm{T}} \end{Bmatrix} \tag{17}$$

is computed from the first column of $\mathbf{Y}^{(i-1)}$ and

$$\mathbf{B}^{(i-1)} \equiv \begin{Bmatrix} \mathbf{y}_{N-i+1} \\ \mathbf{y}_{N-i+2} \\ \vdots \\ \mathbf{y}_{N-1} \end{Bmatrix} \begin{Bmatrix} \mathbf{y}_{N-2i+2}^{\mathrm{T}} & \mathbf{y}_{N-2i+3}^{\mathrm{T}} & \cdots & \mathbf{y}_{N-i}^{\mathrm{T}} \end{Bmatrix} \tag{18}$$

is determined from the last column of $\mathbf{Y}^{(i-1)}$.

3.2 Recursive algorithm and its computation efficiency

Based on Eq. (16), it is apparent that $\hat{\mathbf{T}}^{(i-1)}$ can be efficiently obtained if $\hat{\mathbf{T}}^{(i)}$ is available. This crucial relationship naturally leads to a recursive algorithm for expediently establishing an alternative stabilization diagram in the range from $i = i_{\min}$ to $i = i_{\max} = i_{\min} + \Delta i$. More specifically, this algorithm should start from the

computation of $\hat{\mathbf{T}}^{(i_{\max})}$ and the subsequent approximate Toeplitz matrices corresponding to smaller values of i can then be recursively obtained by Eq. (16) without going through the enormous computation shown in Eq. (9). In fact, even $\hat{\mathbf{T}}^{(i_{\max})}$ does not have to be determined by Eq. (9) if the property of Eq. (15) is applied. Merely the first row of submatrices ($\hat{\mathbf{H}}_{i,0}^{(i)}, \hat{\mathbf{H}}_{(i-1),1}^{(i)}, \cdots\cdots, \hat{\mathbf{H}}_{1,(i-1)}^{(i)}$) and the first column of submatrices ($\hat{\mathbf{H}}_{(i+1,0)}^{(i)}, \hat{\mathbf{H}}_{(i+2),0}^{(i)}, \cdots\cdots, \hat{\mathbf{H}}_{(2i-1),0}^{(i)}$) in Eq. (9) need to be laboriously calculated. The other rows of submatrices for $\hat{\mathbf{T}}^{(i_{\max})}$ can be sequentially obtained by Eq. (15) with very minor computational cost. Moreover, the computation of $\mathbf{F}^{(i-1)}$ and $\mathbf{B}^{(i-1)}$ in Eq. (16) can also be simplified with the use of $\mathbf{F}^{(i)}$ and $\mathbf{B}^{(i)}$. This part of computational cost, however, is trivial compared to the calculation of the Toeplitz matrix. Consequently, such an effort is not further made in this study to keep a concise formulation.

According to the above discussions, a recursive algorithm is developed in this research with the following procedures divided into two parts:

(I) Start from $i = i_{\max}$ to calculate $\hat{\mathbf{T}}^{(i)}$ with three successive steps:

(a) Compute $\hat{\mathbf{H}}_{i,0}^{(i)}, \hat{\mathbf{H}}_{(i-1),1}^{(i)}, \cdots\cdots, \hat{\mathbf{H}}_{1,(i-1)}^{(i)}$ and $\hat{\mathbf{H}}_{(i+1,0)}^{(i)}, \hat{\mathbf{H}}_{(i+2),0}^{(i)}, \cdots\cdots, \hat{\mathbf{H}}_{(2i-1),0}^{(i)}$ directly by the formula of Eq. (10);

(b) Use Eq. (15) to determine the remaining submatrices by

$$\hat{\mathbf{H}}_{(2i-2),0}^{(i)} \rightarrow \hat{\mathbf{H}}_{(2i-2),1}^{(i)}$$
$$\hat{\mathbf{H}}_{(2i-3),0}^{(i)} \rightarrow \hat{\mathbf{H}}_{(2i-3),1}^{(i)} \rightarrow \hat{\mathbf{H}}_{(2i-3),2}^{(i)}$$
$$\vdots$$
$$\hat{\mathbf{H}}_{i,0}^{(i)} \rightarrow \hat{\mathbf{H}}_{i,1}^{(i)} \rightarrow \cdots\cdots \rightarrow \hat{\mathbf{H}}_{i,(i-1)}^{(i)}$$
$$\hat{\mathbf{H}}_{(i-1),1}^{(i)} \rightarrow \hat{\mathbf{H}}_{(i-1),2}^{(i)} \rightarrow \cdots\cdots \rightarrow \hat{\mathbf{H}}_{(i-1),(i-1)}^{(i)}$$
$$\hat{\mathbf{H}}_{(i-2),2}^{(i)} \rightarrow \hat{\mathbf{H}}_{(i-2),3}^{(i)} \rightarrow \cdots\cdots \rightarrow \hat{\mathbf{H}}_{(i-2),(i-1)}^{(i)}$$
$$\vdots$$
$$\hat{\mathbf{H}}_{2,(i-2)}^{(i)} \rightarrow \hat{\mathbf{H}}_{2,(i-1)}^{(i)}$$

(c) Construct $\hat{\mathbf{T}}^{(i)}$ with all the obtained submatrices by Eq. (9).

(II) Apply Eq. (16) to evaluate $\mathbf{T}^{(i_{\max}-1)}, \mathbf{T}^{(i_{\max}-2)}, \cdots\cdots, \mathbf{T}^{(i_{\max}-\Delta i+1)}$ and $\mathbf{T}^{(i_{\max}-\Delta i)} = \mathbf{T}^{(i_{\min})}$ in sequence for performing the subsequent SVD operation in the SSI analysis.

The computational cost for the covariance-driven SSI analysis principally comes from the construction of Hankel matrix expressed in Eq. (3), the determination of the approximate Toeplitz matrix expressed in Eq. (4), and the SVD operation expressed in Eq. (5). Typically, as will be shown in the demonstrative examples in Section 4, the computation times corresponding to these three major operations in the SSI analysis follow the decreasing order of approximate Toeplitz matrix, Hankel matrix, and SVD. Basically, the construction of Hankel matrix is not necessary and the corresponding computation can be avoided by assembling the approximate Toeplitz matrix directly from the output vectors at different time instants. The recursive algorithm proposed in this section further deal with the most time-consuming part in forming the approximate Toeplitz matrix. With Part (I) of this algorithm, the approximate Toeplitz matrix containing a total number of $(i-1)^2$ submatrices can be essentially obtained by generating only $(2i-1)$ of these $l \times l$ submatrices $\hat{\mathbf{H}}_{m,p}^{(i)}$. Part (II) of the recursive algorithm, on the other hand, is particularly designed for the alternative stabilization diagram such that the approximate Toeplitz matrix need to be actually evaluated merely for the maximum considered value of the time lag parameter. In other words, the computation cost for the two most dominant operations in constructing the alternative stabilization diagram can be significantly reduced with the developed approach. However, the SVD operation is still required for each different value of i.

4. Identification of modal parameters for the investigated structure

4.1 Investigated structures and measurements

The recursive algorithm established in the previous section would substantially improve the feasibility of applying the alternative stabilization diagram for conducting a robust SSI analysis in long-term monitoring of civil structures. The investigation in this research is focused on Central Taiwan Science Park Bureau (CTSPB) Building and Industrial & Commercial (IC) Building, which are twin office buildings situated in Central Taiwan Science Park of Taichung. Both CTSPB Building and IC Building are steel framed structures, but the former has 13 stories with a height of 58 m and the latter has 9 stories with a height of 41 m. As illustrated in Fig. 1, the lowest three overground stories and the two underground stories of these two buildings are linked by a common RC structure with a considerably higher rigidity. A long-term monitoring system was installed on these two buildings by National Center of Research on Earthquake Engineering (NCREE) and started its operation at the end of 2015. As also depicted in Fig. 1(a), the high-accuracy MEMS capacitive accelerometers SDI2210-002 manufactured by Silicon Designs, Inc. were deployed at the four positions labeled A, B, C, and D on each of the higher monitored stories. For the lower monitored stories below 4F, the sensors were only placed at A and D. As shown in Fig. 1(b), at least two accelerometers were mounted at each sensor location to take the vibration signals in the long (x) and short (y) directions. One extra accelerometer was supplemented on B2F, 3F, and the top story of each building to measure the response in the vertical (z) direction. Further details regarding these two buildings and the monitoring system can be referred to a recent work (Wu *et al.* 2017c) by the authors and would not be repeated herein.

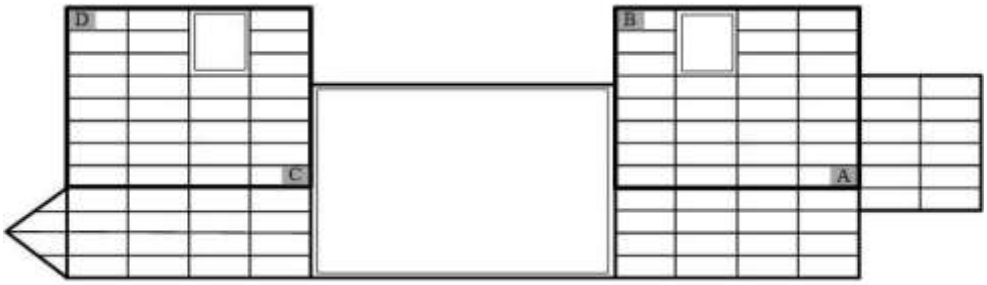

(a) Top view

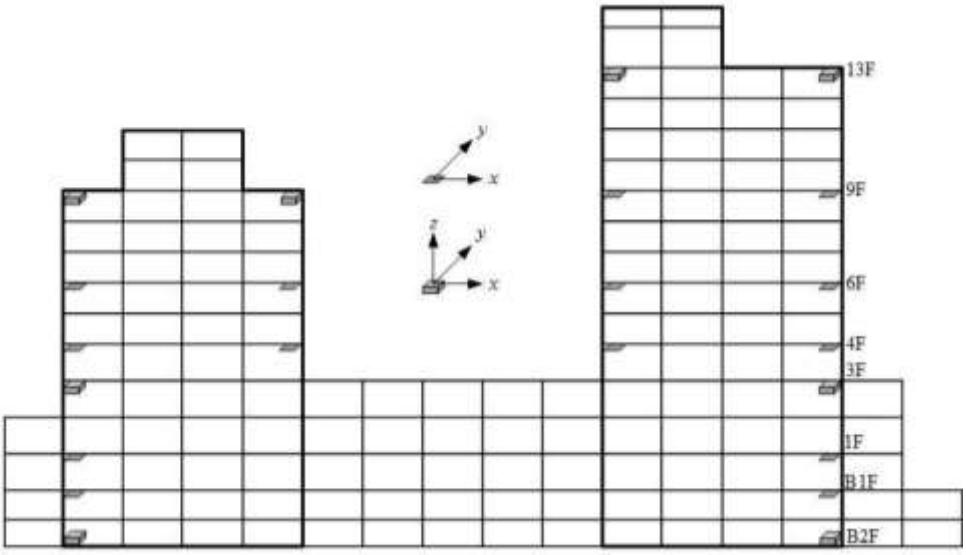

(b) Side view

Fig. 1 CTSPB Building and IC Building with sensor deployment

According to the observations that the responses of the underground stories and those in the vertical direction are generally negligible, the measurements in the *x* and *y* directions no lower than 3F are adopted for more efficient analysis. All these signals collected at a sampling rate of 200 Hz for 20 months from January of 2016 to August of 2017 are examined. Each set of acceleration measurements were automatically output by the monitoring system every 30 minutes. Equally dividing each data set into two with a half of time length, the subsequent SSI analysis is performed to identify one set of modal parameters every 15 minutes. Moreover, these two buildings are eligible to be individually analyzed because the structures above 3F are completely separated and their connected lower parts are relatively rigid. It should be further noticed that the monitoring system experienced several technical problems during these 20 months and the collection of data was interrupted on 24 February, on 9 March, on 21 March, from 22 March to 23 March, on 22 April, on 26 April, from 26 July to 12 August, and from 13 September to 20 October in the year of 2016 and from 7 June to 13 June and from 22 July to 24 July in the year of 2017.

4.2 Alternative stabilization diagram and computation comparison

Taking the measurements from 10:00 to 10:15 on 5 January of 2017 for both buildings as an example, the SSI analysis equipped with the recursive algorithm developed in the previous section is performed to construct the corresponding alternative stabilization diagrams as displayed in Fig. 2. Since only the first few stable modes are concerned for long-term monitoring in this study, the investigation concentrates on the frequency range from 0 to 3 Hz and the analyzed signals are further down-sampled to 100 Hz due to computational consideration. Furthermore, the system order of $n=10$ is fixed for both buildings because around 4 to 5 peaks can be observed in the interested frequency range from the corresponding FAS's. With the fundamental frequency $f_1 \approx 0.75\,\text{Hz}$ for CTSPB Building and $f_1 \approx 1.1\,\text{Hz}$ for IC Building, the critical threshold can be determined according to Eq. (8) as either $i_c = 100/0.75 \approx 133$ or $i_c = 100/1.1 \approx 90$. Further inspecting the actual frequency stability, it is found that $i=85$ can work very well for both cases. To balance the identification accuracy and the computation efficiency in long-term monitoring, the SSI analysis is carried out with

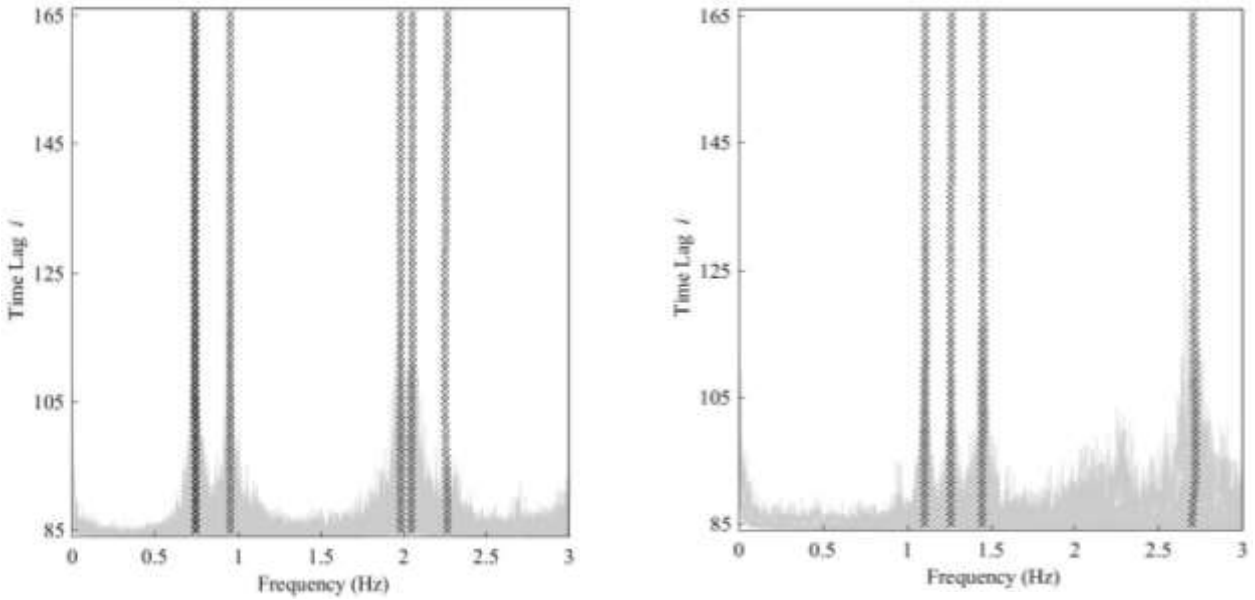

(a) CTSPB Building (b) IC Building

Fig. 2 Alternative stabilization diagrams for CTSPB Building and IC Building

the time lag parameter increasing from $i_{\min}=85$ to $i_{\max}=i_{\min}+\Delta i=85+80=165$ for establishing the alternative stabilization diagrams as in Figs. 2(a) and 2(b). The cross signs are employed in these figures to symbolize the identified frequency values and the corresponding FAS is plotted in the background.

The above example is analyzed by a computer code developed with MATLAB and run on a desktop personal computer. Comparison of the computation times for the three major operations in the SSI analysis would clearly demonstrate the excellent efficiency attained by the proposed recursive algorithm. Considering first the case of $i=i_{\max}=165$, the computation times associated with construction of Hankel matrix, determination of the approximate Toeplitz matrix, and SVD operation based on the direct algorithm are 4.5 sec, 19.2 sec, and 8.1 sec, respectively, for CTSPB Building. On the other hand, the corresponding values based on the recursive algorithm are 0 sec, 4.9 sec, and 7.7 sec, respectively. As described in Subsection 3.2, the new algorithm does not need to construct Hankel matrix and greatly reduces the computation time for forming the approximate Toeplitz matrix. It is also not surprising that the computation times for SVD operation are similar because no modification is made in this category. For the remaining cases with $85=i_{\min}\le i\le i_{\max}-1=164$, the computation cost for the approximate Toeplitz matrix can be nearly neglected in the recursive algorithm with the use of Eq. (16). The total computation time for establishing the alternative stabilization diagram is then examined to evaluate the overall efficiency of the recursive algorithm. For CTSPB Building, the total computation time is 1478 sec with the direct algorithm and 251 sec with the recursive algorithm. The corresponding values for IC Building are 1068 sec and 173 sec, respectively.

The total computation time is apparently reduced to about one sixth with the new recursive algorithm for both buildings. Moreover, the computer memory required to run the SSI analysis is 2.1 GB for the recursive algorithm, compared to 10.4 GB for the direct algorithm. It is noteworthy that the computation involved with the sifting process for the identification of modal parameters as will be described in the next subsection is minor with the computer time less than 1 sec. Accordingly, the application of the recursive algorithm makes it possible to finish the overall analysis on the measurements with a length of 15 minutes within 5 minutes for CTSPB Building and within 3 minutes for IC Building.

4.3 Identified modal parameters and their characteristics

With the stable frequencies efficiently provided by the alternative stabilization diagram, a robust process consisting of three hierarchical sifting stages to extract the close values in all the 3 caterories of modal parameter including frequencies, damping ratios, and mode shape vectors was further developed by the authors in recent works (Wu *et al.* 2016a, Wu *et al.* 2019). Similar procedures were applied with modified parameters in a more recent study (Wu *et al.* 2017c) for investigating CTSPB Building and IC Building. Therefore, the details of this hierarchical sifting process would not be repeated in the current paper. Simply the modal parameters identified from the exemplified measurements mentioned in the previous subsection are presented in this subsection to illustrate the dynamic characteristics of the dominant modes for CTSPB Building and IC Building.

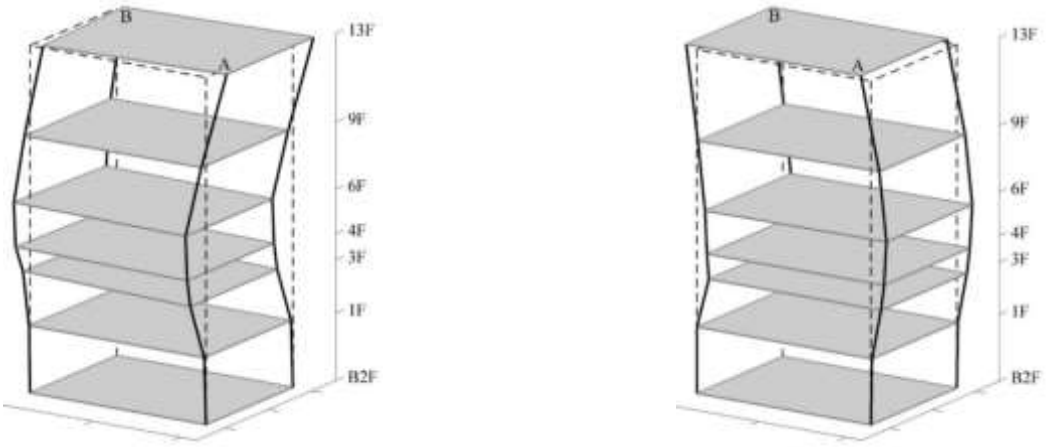

(a) Mode B2-1 (b) Mode B2-2

Fig. 3 Normalized mode shapes of the second pair of bending modes for CTSPB Building

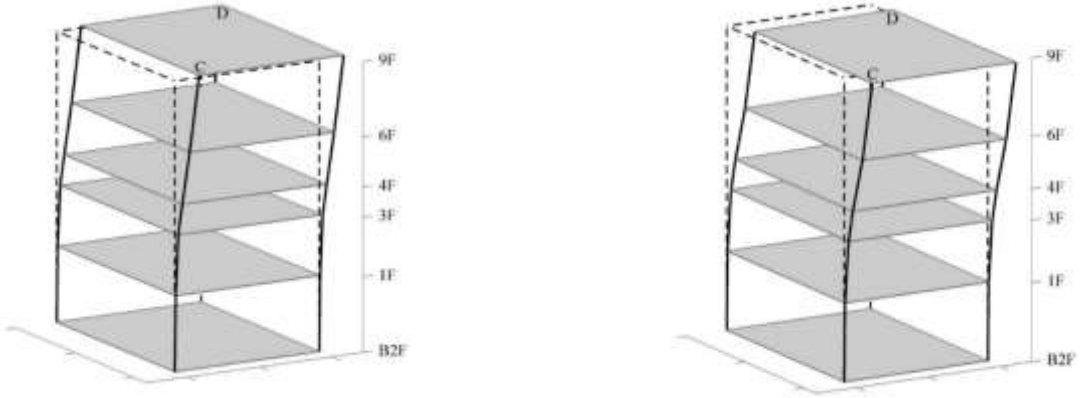

(a) Mode B2-1 (b) Mode B2-2

Fig. 4 Normalized mode shapes of the first pair of bending modes for IC Building

In the first stage of sifting process, six groups of clustered frequency values can be extracted from Fig. 2(a) and four groups from Fig. 2(b). It needs to be emphasized that there actually exist two pairs of closely-spaced modes (Wu *et al.* 2019) in Fig. 2(a) with the frequency values in the neighborhood of 0.75 Hz and 2 Hz, respectively. The second stage is then conducted to sift the close damping ratios for each mode, followed by the third sifting stage for inspecting the consistency of the corresponding mode shape vectors. The modal frequencies, damping ratios, and mode shape vectors surviving all the three stages in each clustered group can be finally averaged to determine the identified modal parameters for each mode. The frequencies and damping ratios of the six identified modes for CTSPB Building and those of the four identified modes for IC Building are listed in Table 1. Besides, the identified mode shapes of the second pair of close modes for CTSPB Building are demonstrated in Fig. 3 with 3D illustrations. Similarly, the 3D mode shapes of the first pair of close modes for IC Building are also depicted in Fig. 4. The reason to particularly plot these two pairs of mode shapes is because they will be chosen to serve as the target modes for long-term monitoring.

Table 1 Identified modal frequencies and damping ratios for CTSPB and IC Building

Building	Mode	Frequency (Hz)	Damping ratio (%)
CTSPB	B1-1	0.742	1.648
	B1-2	0.747	0.926
	T1	0.950	0.962
	B2-1	1.982	1.164
	B2-2	2.053	1.463
	T2	2.260	2.022
IC	B1-1	1.108	1.372
	B1-2	1.263	1.031
	T1	1.450	1.338
	B2	2.706	1.708

From the upper half of Table 1 and Fig. 3 for CTSPB Building, it is clear that the second pair of clustered groups with frequencies 1.982 Hz and 2.053 Hz correspond to two close modes in the second bending mode shape of a conventional building. However, these two modes vibrate

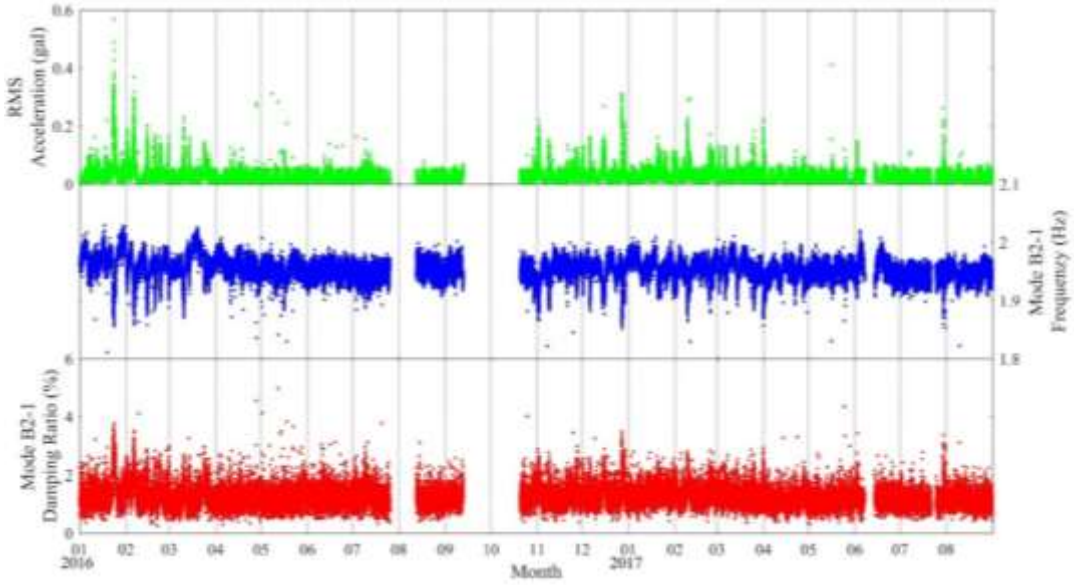

Fig. 5 Comparison of identified modal parameters for Mode B2-1 of CTSPB Building and the RMS acceleration

along two independent directions in the cross-section plane of building and are referred as Modes B2-1 and B2-2, respectively. In fact, the first pair of clustered groups with frequencies 0.742 Hz and 0.747 Hz are also two extremely close modes along independent directions in the first bending mode shape of a conventional building and named Modes B1-1 and B1-2. As for the other two modes with frequencies 0.950 Hz and 2.260 Hz, they are found to be the first two torsional modes and called Mode T1 and Mode T2. From the lower half of Table 1 and Fig. 4 for IC Building, the first two modes with frequencies 1.108 Hz and 1.263 Hz obviously own the first bending mode shape of a building structure along two different directions and are similarly referred as Modes B1-1 and B1-2. The third mode with a frequency of 1.450 Hz and the fourth mode with a frequency of 2.706 Hz are denoted by Modes T1 and B2, respectively, because their mode shapes correspond to be the first torsional mode and the second bending mode of IC Building.

5. Assessment of environmental effects with long-term measurements

The monitoring data of CTSPB Building and IC Building for the first three months of 2016 have been analyzed in a recent study (Wu *et al.* 2017c) to investigate the trend of variation in its modal parameters and evaluate the possible effects from several environmental factors. The environmental factors considered include the air humidity, the wind speed, the air temperature, and the RMS acceleration for each interval to serve as the indication of structural response level. A particularly important discovery was that the RMS response is the most influential quantity on the variation of modal parameters. Cross-examination of these results also disclosed that the RMS vibration responses of both buildings are controlled by the excitation intensity coming from two major sources. The excitation is primarily induced by the live personnel load under a lower wind speed, while the wind speed becomes a much more crucial factor to alter the excitation intensity in the case of strong wind. Most of the modal frequencies were found to highly correlate with the RMS acceleration in a negative manner and the corresponding damping ratios also demonstrated a positive correlation. Statistical analysis was further performed in the same study to determine that Mode B2-1 is the most stable mode (identification percentage > 99%) for CTSPB Building. As for the IC Building, both Modes B1-1 and B1-2 (identification percentage > 99%) play similar roles.

Furnished with the recursive algorithm developed in the current study to more efficiently conduct the SSI analysis, the above work is extended to cover 20 months of monitoring data in this section for more comprehensive investigation. Except for several intervals without signals due to technical problems, there are totally 51833 sets of vibration measurements with a length of 15 minutes to be analyzed in this study. Similar to the statistics in the previous work (Wu *et al.* 2017c), Mode B2-1 owns the best identifiability percentage of 98.5% (51041/51833) for CTSPB Building and Mode B1-2 for IC Building tops the other modes with an identifiability percentage of 98.3% (50953/51833). As a result, Mode B2-1 of CTSPB Building and Mode B1-2 of IC Building are taken to serve as the tracking modes for long-term monitoring. Further considering the most dominant component associated with Mode B2-1 of CTSPB Building, the standard deviation of the measurement along the short (y) direction of the top floor at location A is adopted to stand for the RMS acceleration in this case. With similar reasons, the measurement along the long (x) direction of the top floor at location D is utilized in the case of IC Building to determine the representative RMS acceleration.

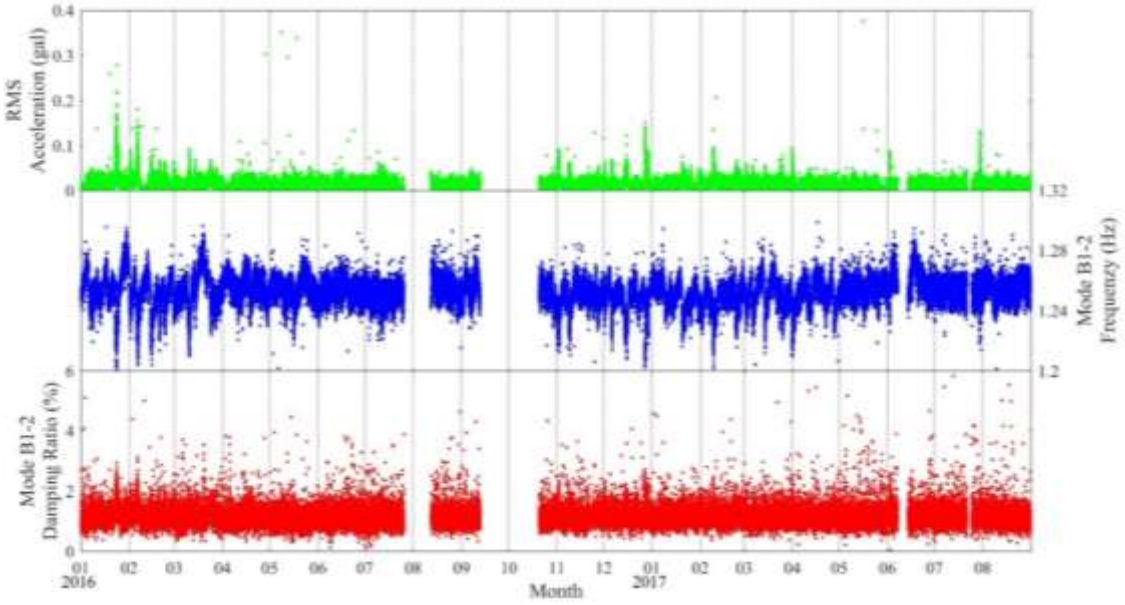

Fig. 6 Comparison of identified modal parameters for Mode B1-2 of IC Building and the RMS acceleration

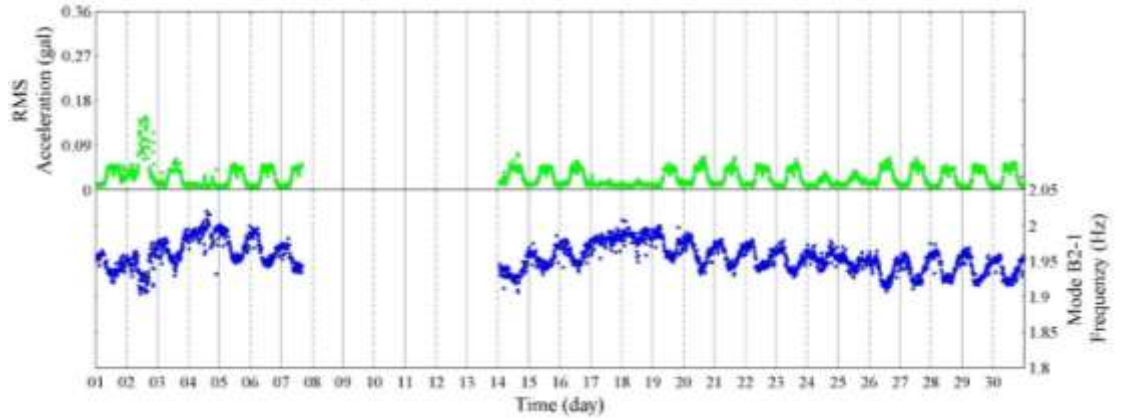

Fig. 7 Comparison of identified frequency for Mode B2-1 of CTSPB Building and RMS acceleration in June of 2017

The modal parameters for the target mode of each building are continuously identified for the observed 20 months to extensively compare with the corresponding variation of RMS acceleration. Based on these results, the variation of RMS acceleration is plotted in Fig. 5 together with those of frequencies and damping ratios for Mode B2-1 in the case of CTSPB Building. Similar comparison is also made for Mode B1-2 of IC Building and illustrated in Fig. 6. From Figs. 5 and 6, it is no doubt that the negative correlation between the target frequency of each building and the corresponding RMS acceleration is strongly held all the year round without any exception. Such a significant effect of the RMS response on the modal frequencies has been explained in the recent work (Wu *et al.* 2017c) by possible relaxation of boundary conditions and contact conditions between structural members under larger responses to decrease the modal frequencies by the reduction in stiffness. The fact that the same trend is retained all the time as shown by the results for 20 months would further confirm the validity of this explanation.

To systematically examine such a tendency in more details, the correlation coefficient is then determined month by month. Although the collection of data was interrupted by technical problems a few times during the total duration of 20 months, it is fortunate that at least 10 days of continuous data can still be extracted in each month to provide a sufficient length for the investigation of correlation. Table 2 lists the obtained results for all the 20 months. The monthly correlation coefficient for Mode B2-1 of CTSPB Building ranges from −0.688 to −0.883 and that for Mode B1-2 of IC Building falls between −0.588 and −0.840. This monthly value for Mode B2-1 of CTSPB Building only goes below the magnitude of 0.7 in 1 of 20 months and the corresponding number for Mode B1-2 of IC Building is 5 in 20 months. Comparison of the results between CTSPB Building and IC Building also demonstrates that the correlation coefficient for the target mode of CTSPB Building is higher than that of IC Building all the time. The best correlation coefficient occurred in December of 2016 for both CTSPB Building and IC

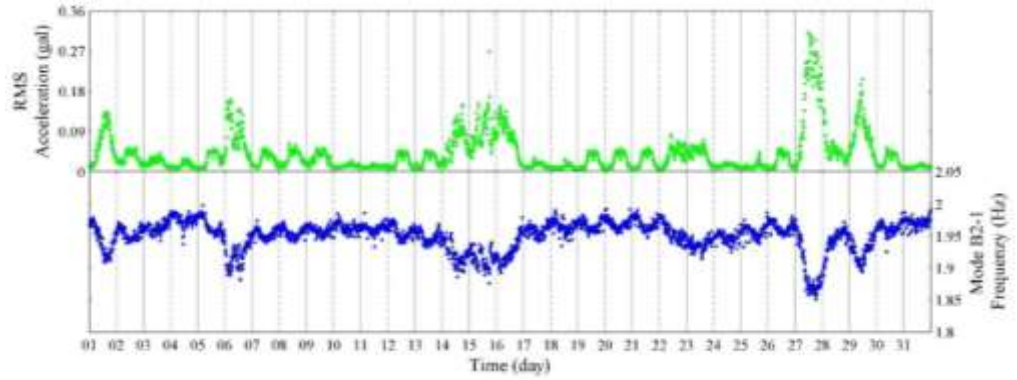

Fig. 8 Comparison of identified frequency for Mode B2-1 of CTSPB Building and RMS acceleration in December of 2016

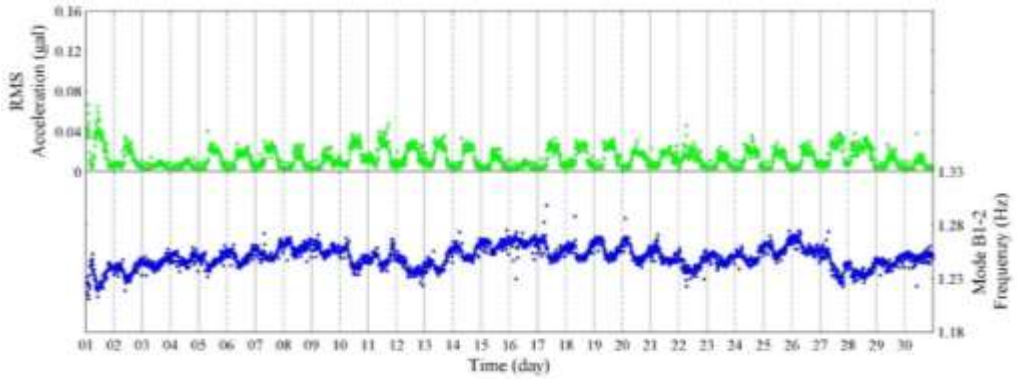

Fig. 9 Comparison of identified frequency for Mode B1-2 of IC Building and RMS acceleration in April of 2017

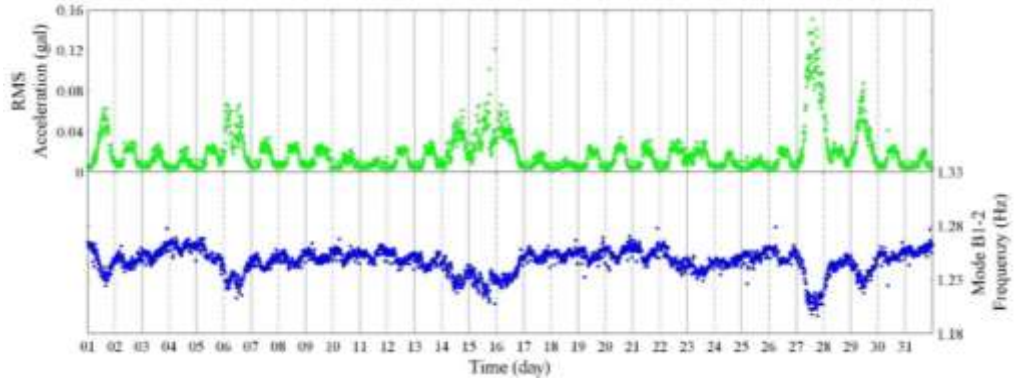

Fig. 10 Comparison of identified frequency for Mode B1-2 of IC Building and RMS acceleration in December of 2016

Building. As for the worst case, it happened in June of 2017 for CTSPB Building and in April of 2017 for IC Building. The variations of RMS acceleration together with those of frequencies in these four extreme cases are magnified in Figs. 7 to 10 for the convenience of closer examination. Because of the technical problem obstructing the data collection from 7 June to 13 June in 2017 as shown in Fig. 7, the correlation coefficient for Mode B2-1 of CTSPB Building in June of 2017 is calculated based on the measurements from 14 June to 30 June. In contrast to Fig. 8 for the case with the highest correlation coefficient, careful inspection of Fig. 7 reveals that the deteriorated value of correlation coefficient in this case is likely due to its lack of larger fluctuations in either modal frequency or RMS acceleration. This conjecture can be further verified by observing the similar trend in Figs. 9 and 10 for Mode B1-2 of IC Building.

Table 2 Correlation coefficient between the target modal frequency and the RMS acceleration

Year	Month	Covered dates	Correlation coefficient with RMS acceleration	
			Mode B2-1 of CTSPB	Mode B1-2 of IC
2016	January	1/1 to 1/31	–0.816	–0.711
	February	2/1 to 2/24	–0.779	–0.762
	March	3/9 to 3/21	–0.792	–0.651
	April	4/1 to 4/22	–0.726	–0.717
	May	5/1 to 5/31	–0.780	–0.726
	June	6/1 to 6/30	–0.793	–0.743
	July	7/1 to 7/26	–0.849	–0.815
	August	8/12 to 8/31	–0.816	–0.745
	September	9/1 to 9/13	–0.836	–0.789
	October	10/20 to 10/31	–0.867	–0.805
	November	11/1 to 11/30	–0.867	–0.827
	December	12/1 to 12/31	–0.883	–0.840
2017	January	1/1 to 1/31	–0.764	–0.658
	February	2/1 to 2/28	–0.880	–0.804
	March	3/1 to 3/31	–0.774	–0.652
	April	4/1 to 4/30	–0.713	–0.588
	May	5/1 to 5/31	–0.831	–0.753
	June	6/14 to 6/30	–0.688	–0.669
	July	7/1 to 7/22	–0.854	–0.823
	August	8/1 to 8/31	–0.795	–0.793

Table 3 Variation of targeted modal frequencies for CTSPB Building and IC Building

Interval	Target mode and building	Average (Hz)	Variation range (Hz)	Variation percentage (%)
2016/1 to 2016/12	B2-1 of CTSPB	1.955	0.208	10.6
	B1-2 of IC	1.252	0.131	10.5
2016/1 to 2017/8	B2-1 of CTSPB	1.953	0.208	10.6
	B1-2 of IC	1.252	0.134	10.7

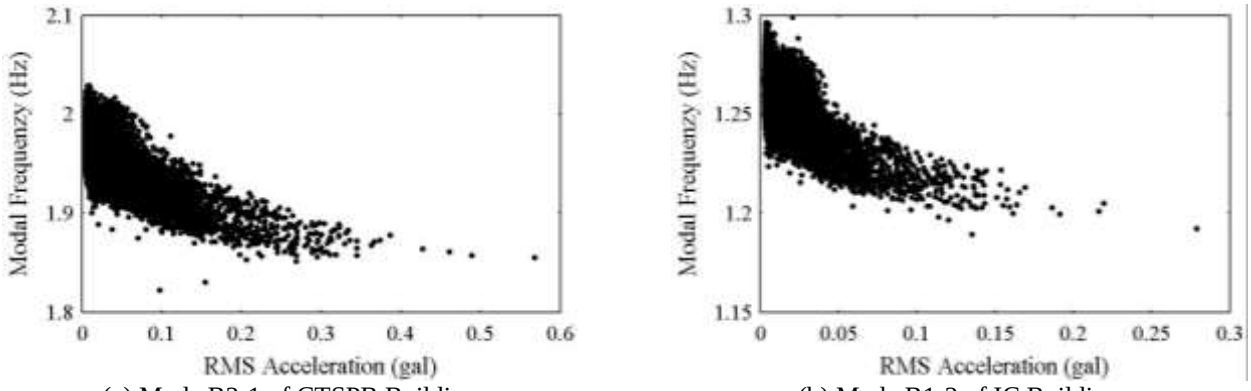

(a) Mode B2-1 of CTSPB Building (b) Mode B1-2 of IC Building

Fig. 11 Modal frequency versus RMS acceleration for the target mode

The range of modal frequency variation under normal environmental conditions is usually of general concerns in structural health monitoring and damage detection. The average, range of variation (difference between the maximum and minimum values), and percentage of variation (range of variation divided by the average) in either the 12 months of 2016 or all the 20 months from 2016 to 2017 are listed in Table 3 for Mode B2-1 of CTSPB Building and Mode B1-2 of IC Building. From Table 3, it is clear that the percentages of frequency variation for the target modes of both CTSPB Building and IC Building are around 11% in the whole year of 2016. Furthermore, the average, variation range, and variation percentage are found to be almost unchanged if the inspection interval is extended to include 8 more months in 2017. This phenomenon indicates the variations of modal frequencies for both buildings are quite stable and the measurements covering one whole year would be sufficient for conducting a representative investigation. Finally, the plots of targeted modal frequency versus RMS acceleration to cover all the results in 20 months are displayed in Fig. 11 for both buildings. Other than showing the frequency values to generally decrease with the increasing RMS acceleration, Fig. 11 further illustrates that this relationship seems not to be totally linear. More specifically, the magnitude for the negative slope of this relationship tends to decrease with the RMS acceleration and an exponential function may be more appropriate for filtering out the effect of response level on the modal frequencies.

6. Conclusions

To enhance the computation efficiency of a recently proposed SSI methodology based on the alternative stabilization diagram, this research develops a novel recursive algorithm such that the most computation-consuming operation for obtaining the approximate Toeplitz matrix does not have to be repeated for each value of time lag parameter. The similarity in the submatrices of the two approximate Toeplitz matrices corresponding to adjacent values of time lag parameter is analytically explored to derive a recursive formula. It is suggested that the recursive algorithm should start from maximum value of time lag parameter and the approximate Toeplitz matrix in this case can basically be determined by only calculating the first row and the first column of submatrices according to another derived relationship between the submatrices. Exemplified by the measurements taken from the two investigated office buildings, it is demonstrated that merely one sixth of computation time and one fifth of computer memory are needed with the new recursive algorithm. This critical progress would enable the realization of on-line and almost real-time monitoring for these two steel framed structures with a personal computer.

The established recursive SSI algorithm is further applied to expediently analyze 20 months of monitoring data collected from the two office buildings and comprehensively assess the environmental effects. Focused on the most stably identified mode for each building and taking the standard deviation of the acceleration measurement for its most dominant component to represent the RMS vibration response, it is thoroughly certified that the RMS response can be utilized as an excellent index to represent most of the environmental effects and its variation strongly correlates with that of the modal frequency in a negative manner. More detailed examination by comparing the monthly correlation coefficient discloses that larger variations in modal frequency induced by greater RMS responses would typically lead to a higher correlation. In addition, this correlation is also found to be relatively weaker for the shorter of the two inspected buildings. Another important information gained from the investigation is that the percentages of frequency variation for the target modes of both buildings are approximately 11% in either the whole year of 2016 or for all the 20 months to indicate the consistency of long-term monitoring.

Based on the convincing assessment in the current study to validate the dominant influence of the RMS response on the modal frequency of a steel framed structure, the subsequent work to exclude its interference from the variation of the targeted modal frequency for constructing a sensitive damage detection method is underway. Such an elimination is relatively convenient in the considered case because the RMS response can be directly obtained from the vibration signals without any extra measurements. A valuable observation from this work that the negative slope of the modal frequency to decrease with the increasing RMS acceleration is not constant would also provide an instructive clue to adopt an exponential function for a more effective filtering. Regarding the future development of a potentially more efficient SSI algorithm based on the alternative stabilization diagram, attempts are also made to search for the possibility in simplifying the SVD operations associated with each different value of time lag parameter.

Acknowledgments

The authors are grateful to the financial support from the Ministry of Science and Technology of Republic of China under Grant MOST105-3011-F-009-003 and Grant MOST106-3011-F-009-003.

References

Amezquita-Sanchez, J.P. and Adeli, H. (2016), "Signal processing techniques for vibration-based health monitoring of structures", *Arch. Comput. Method Eng.*, **23**(1), 1-15. https://doi.org/10.1007/s11831-014-9135-7.

Apaydin, N.M., Kaya, Y., Safak, E. and Alcik, H. (2012), "Vibration characteristics of a suspension bridge under traffic and no traffic conditions", *Earthq. Eng. Struct. D.*, **41**(12), 1717-1723. https://doi.org/10.1002/eqe.1196.

Bakir, P.G. (2011), "Automation of the stabilization diagram for subspace based system identification", *Exp. Syst. Appl.*, **38**(12), 14390-14397. https://doi.org/10.1016/j.eswa.2011.04.021.

Belleri, A., Moaveni, B. and Restrepo, J.I. (2014), "Damage assessment through structural identification of a three-story large-scale precast concrete structure", *Earthq. Eng. Struct. D.*, **43**(1), 61-76. https://doi.org/10.1002/eqe.2332.

Cao, Y.H., Yim, J.S., Zhao, Y. and Wang, M.L. (2011), "Temperature effects on cable stayed bridge using health monitoring system: a case study", *Struct. Health Monit.*, **10**(5), 523-537. https://doi.org/10.1177/1475921710388970.

Carden, E.P. and Brownjohn J.M. (2008), "Fuzzy clustering of stability diagrams for vibration-based structural health monitoring", *Comput.-Aided Civil Infrastruct. Eng.*, **23**(5), 360-372. https://doi.org/10.1111/j.1467-8667.2008.00543.x.

Faheem, B. and Piotr, O. (2014), "Seismic response trends evaluation and finite element model calibration of an instrumented RC building considering soil-structure interaction and non-structural components", *Eng. Struct.*, **65**, 111-123. https://doi.org/10.1016/j.engstruct.2014.01.045.

Faravelli, L., Ubertini, F. and Fuggini, C. (2011), "System identification of a super high-rise building via a stochastic subspace approach", *Smart Struct. Syst.*, **7**(2), 133-152. https://doi.org/10.12989/sss.2011.7.2.133.

Foti D., Gattulli V. and Potenza F. (2014) "Output-only identification and model updating by dynamic testing in unfavorable conditions of a seismically damaged building", *Comput.-Aided Civil Infrastruct. Eng.*, **29**(9), 659-675. https://doi.org/10.1111/mice.12071.

Gentile, C. and Saisi, A. (2013), "Operational modal testing of historic structures at different levels of excitation", *Constr. Build. Mater.*, **48**, 1273-1285. https://doi.org/10.1016/j.conbuildmat.2013.01.013.

He X., Moaveni B., Conte J.P. and Elgamal A. (2008), "Modal identification study of Vincent Thomas Bridge using simulated wind-induced ambient vibration data", *Comput.-Aided Civil Infrastruct. Eng.*, **23**(5), 373-388. https://doi.org/10.1111/j.1467-8667.2008.00544.x.

Hu, W.H., Chuha, A., Caetano, E., Magalhaes, F. and Moutinho, C. (2010), "LabVIEW toolkits for output-only modal identification and long-term dynamic structural monitoring", *Struct. Infrastruct. Eng.*, **6**(5), 557-574. https://doi.org/10.1080/15732470903068672.

Li, Z. and Chang, C.C. (2012), "Tracking of structural dynamic characteristics using recursive stochastic subspace identification and instrumental variable technique", *J. Eng. Mech.-ASCE*, **138**(6), 591-600. https://doi.org/10.1061/(ASCE)EM.1943-7889.0000370.

Li, S.L., Li, H., Liu, Y., Lan, C.M., Zhou, W.S. and Ou, J.P. (2014), "SMC structural health monitoring benchmark problem using monitored data from an actual cable-stayed bridge", *Struct. Control Health Monit.*, **21**(2), 156-172. https://doi.org/10.1142/S0219455416400253.

Liu, Y.C., Loh, C.H. and Ni, Y.Q. (2013), "Stochastic subspace identification for output-only modal analysis: application to super high-rise tower under abnormal loading condition", *Earthq. Eng. Struct. D.*, **42**(4), 477-498. https://doi.org/10.1002/eqe.2223.

Loh, C.H. and Liu, Y.C. (2013), "Application of recursive SSA as data pre-processing filter for stochastic subspace identification", *Smart Struct. Syst.*, **11**(1), 19-34. https://doi.org/10.12989/sss.2013.11.1.019.

Loh, C.H., Weng, J.H., Chen, C.H. and Lu, K.C. (2013), "System identification of mid-story isolation building using both ambient and earthquake response data", *Struct. Control Health Monit.*, **20**(2), 19-35. https://doi.org/10.1002/stc.479.

Loh, C.H., Weng, J.H., Liu, Y.C., Lin, P.Y. and Huang, S.K. (2011), "Structural damage diagnosis based on on-line recursive stochastic subspace identification", *Smart Mater. Struct.*, **20**(5), 055004. https://doi.org/10.1088/0964-1726/20/5/055004.

Lorenzoni, F., Casarin, F., Caldon, M., Islami, K. and Modena, C. (2016), "Uncertainty quantification in structural health monitoring: applications on cultural heritage buildings", *Mech. Syst. Sig. Pr.*, **66-67**, 268-281. https://doi.org/10.1016/j.ymssp.2015.04.032.

Macdonald, J.H.G. and Daniell, W.E. (2005), "Variation of modal parameters of a cable-stayed bridge identified from ambient vibration measurements and FE modelling", *Eng. Struct.*, **27**(13), 1916-1930. https://doi.org/10.1016/j.engstruct.2005.06.007.

Magalhaes, F., Cunha, A. and Caetano, E. (2009), "Online automatic identification of the modal parameters of a long span arch bridge", *Mech. Syst. Signal Pr.*, **23**, 316-329. https://doi.org/10.1016/j.ymssp.2008.05.003.

Min, Z., Sun, L. and Dan, D. (2009), "Effect analysis of environmental factors on structural modal parameters of a cable-stayed bridge", *J. Vib. Shock*, **28**(10), 99-105.

Nayeri, R.D., Masri, S.F., Ghanem, R.G. and Nigbor, R.L. (2008), "A novel approach for the structural identification and monitoring of a fullscale 17-story building based on ambient vibration measurements", *Smart Mater. Struct.*, **17**(2), 1-19. https://doi.org/10.1088/0964-1726/17/2/025006.

Peeters, B. (2000), "System identification and damage detection in civil engineering", Ph.D. Dissertation, Katholieke Universiteit Leuven, Leuven.

Ramos, L.F., Marques, L., Lourenco, P.B., De Roeck, G., Campos-Costa, A. and Roque, J. (2010), "Monitoring historical masonry structures with operational modal analysis: two cases studies", *Mech. Syst. Signal Pr.*, **24**(5), 1291-1305. https://doi.org/10.1016/j.ymssp.2010.01.011.

Reynders, E. and De Roeck, G. (2008), "Reference-based combined deterministic-stochastic subspace identification for experimental and operational modal analysis", *Mech. Syst. Sig. Pr.*, **22**(3), 617-637. https://doi.org/10.1016/j.ymssp.2007.09.004.

Reynders, E., Houbrects, J. and De Roeck, G. (2012), "Fully automated (operational) modal analysis", *Mech. Syst. Signal Pr.*, **29**, 228-250. https://doi.org/10.1016/j.ymssp.2012.01.007.

Saisi, A., Gentile, C. and Guidobaldi, M. (2015), "Post-earthquake continuous dynamic monitoring of the Gabbia Tower in Mantua, Italy", *Constr. Build. Mater.*, **81**, 101-112. https://doi.org/10.1016/j.conbuildmat.2015.02.010.

Saisi, A., Guidobaldi, M. and Gentile, C. (2016), "On site investigation and health monitoring of a historic tower in Mantua, Italy", *Appl. Sciences*, **6**(6), 173. https://doi.org/10.3390/app6060173.

Scionti, M. and Lanslots, J.P. (2005), "Stabilisation diagrams: pole identification using fuzzy clustering techniques", *Adv. Eng. Softw.*, **36**(11), 768-779. https://doi.org/10.1016/j.advengsoft.2005.03.029.

Sun, L., Zhou, Y. and Xie, D. (2015), "Periodic characteristics of environmental effects on modal frequencies of a cable-stayed bridge", *J. Tongji U.*, **43**(10), 1454-1462.

Ubertini, F., Comanducci, G., Cavalagli, N., Pisello, A.L., Materazzi, A.L. and Cotana, F. (2017), "Environmental effects on natural frequencies of the San Pietro Bell Tower in Perugia, Italy, and their removal for structural performance assessment", *Mech. Syst. Sig. Pr.*, **82**, 307-322. https://doi.org/10.1016/j.ymssp.2016.05.025.

Ubertini, F., Gentile, C. and Materazzi, A.L. (2013), "Automated modal identification in operational conditions and its application to bridges", *Eng. Struct.*, **46**, 264-278. https://doi.org/10.1016/j.engstruct.2012.07.031.

Van Overschee, P. and De Moor, B. (1991), "Subspace algorithm for the stochastic identification problem", *Proceedings of the 30th IEEE Conference on Decision and Control*, Brighton, England, December.

Van Overschee, P. and De Moor, B. (1993), "Subspace algorithms for the stochastic identification problem", *Automatica*, **29**(3), 649-660. https://doi.org/10.1016/0005-1098(93)90061-W.

Van Overschee, P. and De Moor, B. (1996), *Subspace*

Identification for Linear Systems: Theory-Implementation-Applications, Kluwer Academic Publishers, Dordecht, Netherlands.

Weng, J.H. and Loh, C.H. (2011), "Recursive subspace identification for on-line tracking of structural modal parameter", *Mech. Syst. Signal Pr.*, **25**(8), 2923-2937. https://doi.org/10.1016/j.ymssp.2011.05.013.

Westgate, R., Koo, K.Y. and Brownjohn, J. M. W. (2015), "Effect of vehicular loading on suspension bridge dynamic properties", *Struct. Infrastruct. Eng.*, **11**(2), 129-144. https://doi.org/10.1080/15732479.2013.850731.

Whelam, M.J. and Janoyan, K.D. (2010), "In-service diagnostics of a highway bridge from a progressive damage case study", *J Bridge Eng. - ASCE*, **15**(5), 597-607. https://doi.org/10.1061/(ASCE)BE.1943-5592.0000088.

Wu, W.H., Chen, C.C., Shi, W.S. and Huang, C.M. (2017b), "Assessment of environmental effects in scour monitoring of a cable-stayed bridge simply based on pier vibration measurements", *Smart Struct. Syst.*, **20**(2), 231-246. https://doi.org/10.12989/sss.2017.20.2.231.

Wu, W.H., Wang, S.W., Chen, C.C. and Lai, G. (2016a), "Application of stochastic subspace identification for stay cables with an alternative stabilization diagram and hierarchical sifting process", *Struct. Control Health Monit.*, **23**(9), 1194-1213. https://doi.org/10.1002/stc.1836.

Wu, W.H., Wang, S.W., Chen, C.C. and Lai, G. (2016b), "Mode identifiability of a cable-stayed bridge under different excitation conditions assessed with an improved algorithm based on stochastic subspace identification", *Smart Struct. Syst.*, **17**(3), 363-389. https://doi.org/10.12989/sss.2016.17.3.363.

Wu W.H., Wang S.W., Chen C.C. and Lai G. (2017a), "Stable modal identification for civil structures based on a stochastic subspace algorithm with appropriate selection of time lag parameter", *Struct. Monit. Maint.*, **4**(4), 331-350. https://doi.org/10.12989/smm.2017.4.4.331.

Wu, W.H., Wang, S.W., Chen, C.C. and Lai, G. (2017c), "Assessment of environmental and nondestructive earthquake effects on modal parameters of an office building based on long-term vibration measurements", *Smart Mater. Struct.*, **26**(5), 055034. https://doi.org/10.1088/1361-665X/aa6ae6.

Wu, W.H., Wang, S.W., Chen, C.C. and Lai, G. (2019), "Modal parameter identification for closely spaced modes of civil structures based on an upgraded stochastic subspace methodology", *Struct. Infrastruct. Eng.*, **15**(3), 296-313. https://doi.org/10.1080/15732479.2018.1547770.

Yuen, K.V. and Kuok, S. C. (2010), "Ambient interference in long-term monitoring of buildings", *Eng. Struct.*, **32**(8), 2379-2386. https://doi.org/10.1016/j.engstruct.2010.04.012.

Zhang, Q.W., Fan, L.C. and Yuan, W.C. (2002), "Traffic-induced variability in dynamic properties of cable-stayed bridge", *Earthquake Eng. Struct. Dyn.*, **31**(11), 2015-2021. https://doi.org/10.1002/eqe.204.